J. Fluid Mech. (1999), *vol.* 386, *pp.* 233–258. Printed in the United Kingdom

Rayleigh–Bloch surface waves along periodic gratings and their connection with trapped modes in waveguides

By R. PORTER AND D. V. EVANS

School of Mathematics, University of Bristol, Bristol, BS8 1TW, UK

(Received 22 July 1998 and in revised form 26 November 1998)

Rayleigh–Bloch surface waves are acoustic or electromagnetic waves which propagate parallel to a two-dimensional diffraction grating and which are exponentially damped with distance from the grating. In the water-wave context they describe a localized wave having dominant wavenumber β travelling along an infinite periodic array of identical bottom-mounted cylinders having uniform cross-section throughout the water depth. A numerical method is described which enables the frequencies of the Rayleigh–Bloch waves to be determined as a function of β for an arbitrary cylinder cross-section. For particular symmetric cylinders, it is shown how a special choice of β produces results for the trapped mode frequencies and mode shapes in the vicinity of any (finite) number of cylinders spanning a rectangular waveguide or channel. It is also shown how one particular choice of β gives rise to a new type of trapped mode near an unsymmetric cylinder contained within a parallel-sided waveguide with locally-distorted walls. The implications for large forces due to incident waves on a large but finite number of such cylinders in the ocean is discussed.

1. Introduction

In the theory of classical linearized water waves in unbounded domains, there are many situations in which trapped modes exist. Trapped modes describe a localized oscillation having finite energy which exists at some well-defined frequency and which persists for all time in the absence of external forcing, such as an incident wave field. The first example of such a trapped mode was due to Stokes (1846) who constructed a non-trivial solution describing waves travelling along an infinitely-long beach of constant slope, but whose amplitude decays exponentially out to sea. Such a trapped mode has been referred to as an edge wave. Similar edge waves have also been constructed over various sea-bed topographies consisting of local elevations and over submerged horizontal cylinders. A recent review of the various types of trapped modes is given by Evans & Kuznetsov (1997). The crucial ingredient in all these problems is the uniformity of a geometrical cross-section in one of the horizontal coordinates which allows a periodicity to be extracted from the potential in that coordinate. Associated with the periodicity is a wavenumber, k_c, and frequency $\omega_c = (gk_c)^{1/2}$. Simple arguments show that waves cannot radiate to infinity when the frequency of motion, ω, is below ω_c; the waves (if they exist) must be trapped. In such cases, we say that we are operating at a frequency below the cut-off frequency, ω_c. Without the existence of such a cut-off, any wavenumber of motion gives rise to radiated waves. In spectral theory terms, the existence of a trapped mode at a discrete frequency or

wavenumber is equivalent to the existence of an eigenfunction corresponding to a point eigenvalue of the appropriate (unbounded) operator plus boundary conditions. In general, for wave radiation to infinity, the wavenumber spectrum is continuous and given by $k \in [0, \infty)$. However, the geometry has induced a cut-off and the continuous spectrum has been shifted to $k \in [k_c, \infty)$ increasing the possibility of the existence of a trapped mode wavenumber $< k_c$. It should be noted, however, that trapped modes have been discovered having $k > k_c$. See, for example, Evans & Porter (1998).

A different example of trapped modes occurs in consideration of the fluid motion in the vicinity of a single symmetric cylinder of uniform cross-section placed on the centreline of a parallel open-ended channel of uniform width $2d$, say. The existence of such a trapped mode, antisymmetric about the centreline, was first proved by Callan, Linton & Evans (1991) for sufficiently small circular cylinders and subsequently Evans, Levitin & Vassiliev (1994) proved that such trapped modes exist for a wide class of cylinder cross-sections symmetric with respect to the centreline of the channel. The authors were motivated to seek such a trapped mode by the following reasoning. In a channel open-ended at $x = \pm\infty$ containing no obstacle, waves of the form $\mathrm{e}^{\mathrm{i}kx}$, $|x| \to \infty$ are possible for all values of wavenumber k. With k the spectral parameter in this problem, the continuous spectrum is given by $k \in [0, \infty)$. If a symmetric cylinder is now introduced on the centreline of the channel, then it is natural to consider symmetric and antisymmetric problems separately. By choosing the latter of these, and using simple separation of variables far away from the cylinder, it becomes clear that waves can only propagate to infinity if $k > \pi/2d$. Thus, the continuous spectrum for this antisymmetric problem is $k \in [\pi/2d, \infty)$ and one may anticipate discrete values of $k < k_c$ which correspond to trapped modes. It is important to note that these trapped modes are technically still embedded in the full continuous spectrum. However, the decomposition into the antisymmetric part is essential if the existence proof is to succeed. This point will be referred to later.

We shall also be concerned with the case when the Neumann condition on the channel walls (representing no normal flow through the walls) is replaced by the less physical case of a Dirichlet condition. Again, for symmetric cylinders on the centreline, the problem can be decomposed into symmetric and antisymmetric parts. The latter of these again leads to trapped modes since, in this case, the continuous spectrum has been reduced to $k \in [\pi/d, \infty)$. The conditions under which Dirichlet trapped modes exist are not clear; applying the rigorous methods of Evans *et al.* (1994) shows that Dirichlet trapped modes exist if the maximum width of the body is less than or equal to half the width of the channel, though geometries such as circular cylinders increase this ratio to approximately 0.68.

The importance of both Neumann and Dirichlet trapped modes has been brought sharply into focus by a recent paper by Maniar & Newman (1997) who show numerically how large forces on cylinders in the middle of a large but finite array of cylinders can occur at frequencies very close to the corresponding Neumann and Dirichlet trapped modes around a single cylinder in a channel. Such long periodic but finite arrays of cylinders arise in a variety of offshore applications such as, for example, an early design of the proposed offshore runway being developed in Japan. Prompted by this, the present authors (Evans & Porter 1997) recently extended the ideas of Callan *et al.* (1991) to consider the trapped modes which may exist in the vicinity of any number of circular cylindrical cross-sections placed on the centreline of a channel. In general it was found that as many trapped modes existed as there were cylinders present.

Yet another example of trapped modes are Rayleigh–Bloch surface waves which are

closely connected with the Neumann and Dirichlet trapped modes described above as we shall see. Rayleigh–Bloch surface waves in the context of water waves are characterized by a localized wave, having dominant wavenumber β travelling along an infinite periodic linear array of identical vertical cylinders uniform throughout the depth. Removing the depth dependence from the problem reduces the field equation to the two-dimensional Helmholtz equation, and the problem may be regarded as determining the waves along a periodic diffraction grating applicable to the study of optics or along a corrugated surface as in electromagnetics where such waves are described as surface or slow waves.

In the scattering of an incident plane wave by a periodic array of identical cylinders of period $2d$, use is made of the periodicity to argue that the only change in phase in the solution in a displacement $2d$ along the line of cylinders is a multiplier $\mathrm{e}^{2\mathrm{i}\beta d}$ being the change in phase of the incident wave field in such a displacement. Here, $\beta = k\sin\theta$ is the component of the wavenumber of the incident wave in the direction of the line of cylinders and θ is the angle of incident of the plane wave. Clearly k lies in the continuous spectrum $k \in [\beta, \infty)$ and in order to find Rayleigh–Bloch surface waves in the absence of an incident wave or any wave radiation to infinity it is desirable to seek real values of $k < \beta$.

In the context of water waves, Rayleigh–Bloch surface waves have been constructed for specific geometrical configurations such as arrays of thin parallel plates (Evans & Linton 1993), arrays of rectangular blocks (Evans & Fernyhough 1995) and arrays of circular cylinders (McIver, Linton & McIver 1998 and Evans & Porter 1998). In each of these papers, the solutions were constructed numerically and no proofs of existence were provided. In the present paper also, we examine numerically possible geometrical restrictions on the existence of Rayleigh–Bloch surface waves by considering arrays of cylinders having an arbitrary cross-section.

We find that Rayleigh–Bloch surface waves occur for cylinder cross-sections which are symmetric about a line perpendicular to the line through the cylinders. This is consistent with the results of the authors mentioned in the previous paragraph and perhaps not unexpected. However it is also found that, for the specific value $\beta = \pi/2d$, Rayleigh–Bloch surface waves exist about cylinders of arbitrary cross-section and correspond to standing modes. For symmetric cylinder cross-sections this solution is just the Neumann trapped mode in a parallel straight-walled waveguide of width $2d$ described above. For non-symmetric cylinders they may also be regarded as Neumann trapped modes but in a parallel waveguide of width $2d$ which is distorted in the vicinity of the cylinder. This is a new result which has important implications for the forces on a finite but large array of such non-symmetric cylinders.

The problem is formulated in §§ 2 and 3. The method of solution is based upon using an appropriate Green function in Green's Identity to formulate the problem in terms of an integral equation for the potential over a single cylinder boundary. The solution is approximated numerically using a collocation scheme and trapped modes correspond to the zeros of the resulting complex determinant. It turns out that there are two circumstances under which the generally complex determinant can be made real (thus increasing the possibility of the existence of a real zero). The first occurs when the body is symmetric and uses symmetry properties of the Green function. The other relies on the fact that the Green function is real if $\beta = \pi/2d$ or π/d and also leads to a real determinant, but in the case $\beta = \pi/2d$ without making any assumptions on the shape of the cylinder cross-section in doing so.

We present results in § 4 for Rayleigh–Bloch surface waves along arrays of symmetric cylinders, showing the variation of k against β as well as free-surface plots

of various modes. Most importantly, the symmetry in the cylinder cross-sections permits a decomposition of the full potential about any geometric line of symmetry into its symmetric and antisymmetric parts. By considering each of these separately whilst choosing values of $\beta = n\pi/2Nd$, $n = 1,\ldots,N;\ 2N$ one can reconstruct the trapped modes about N equally-spaced identical cylinders spanning symmetrically a waveguide of width $2Nd$ having either Neumann of Dirichlet conditions on the walls, recently described by Utsunomiya & Eatock Taylor (1998) in their numerical treatment of the problem. Thus, for N symmetric cylinders, choosing $N+1$ specific values of Rayleigh–Bloch number β results in $N+1$ distinct values of wavenumber k which in turn leads to at least N Neumann and at most N Dirichlet trapped mode solutions for the corresponding waveguide problem. The advantages of approaching problems involving trapped modes about cylinders spanning the waveguide from a Rayleigh–Bloch perspective are clear. One only has to solve for a single cylinder and apply the appropriate values of β to recover all possible modes, the number and type of modes are easy to identify, and all the trapped mode frequencies are below the Rayleigh–Bloch cut-off frequency, something that is not apparent using other approaches. This allows the solutions to correspond to the vanishing of a real (rather than complex) determinant.

Also, in § 5 we present results for Rayleigh–Bloch waves about unsymmetric cylinders with $\beta d = \frac{1}{2}\pi$ and show how they correspond to trapped modes about cylinders contained within a parallel waveguide distorted locally about the cylinder. The influence of the existence of such a trapped mode on finite periodic arrays of unsymmetric cylinders is demonstrated by the close agreement of numerical results computed by Newman (personal communication) for wavenumbers at which large resonance occurs in the finite array with those computed from our method for the infinite array.

2. Formulation and preliminaries

Consider an infinite array of identical vertical cylinders extending uniformly throughout the depth, $0 \leqslant z \leqslant H$, placed periodically along the y-axis at $(x, y) = (0, 2jd)$, $-\infty < j < \infty$. Let each of the cylinders have the same general cross-section D with boundary given by ∂D.

In classical linearized theory if a time-harmonic motion of radian frequency ω is assumed and the depth dependence removed through a factor $\cosh k(H-z)$, the two-dimensional complex velocity potential for the flow satisfies the Helmholtz equation,

$$(\nabla^2 + k^2)\phi(x, y) = 0, \quad \nabla^2 \equiv \partial_{xx} + \partial_{yy}, \tag{2.1}$$

everywhere in the field apart from on the boundaries of the cylinders where

$$\frac{\partial \phi}{\partial n} = 0, \quad (x, y) \in \partial D \tag{2.2}$$

and n denotes the outward normal derivative with respect to ∂D. Since, for a Rayleigh–Bloch surface wave, the far field vanishes, we impose

$$\phi(x, y) \to 0 \quad \text{as } |x| \to \infty, -\infty < y < \infty. \tag{2.3}$$

Here, k is the real positive root of $\omega^2 = gk \tanh kH$. Because the geometry is periodic, the only change in ϕ in going from a point (x, y) to a point $(x, y + 2d)$, is a change of phase of say $\mathrm{e}^{\mathrm{i}2\beta d}$, where β is a real (Rayleigh–Bloch) wavenumber which can be assumed to be positive. Thus in general we may write

$$\phi(x, y + 2jd) = \mathrm{e}^{\mathrm{i}2\beta dj}\phi(x, y), \quad j = \pm 1, \pm 2, \ldots\ . \tag{2.4}$$

Alternatively we may write

$$\phi(x,y) = \mathrm{e}^{\mathrm{i}\beta y}\widehat{\phi}(x,y) \tag{2.5}$$

where $\widehat{\phi}(x,y)$ is a function periodic in y with period $2d$.

From (2.4) the total field can be obtained by referring to a single strip of width $2d$ containing a cylinder cross-section. We may therefore restrict our attention to the strip $(x,y) \in (-\infty,\infty)\times[-d,d]$ and impose appropriate boundary conditions on the lines $y = \pm d$ expressing the periodicity in (2.4) as

$$\phi(x,d) = \mathrm{e}^{\mathrm{i}2\beta d}\phi(x,-d), \quad \phi_y(x,d) = \mathrm{e}^{\mathrm{i}2\beta d}\phi_y(x,-d) \tag{2.6}$$

with (2.4) then providing the extension to all (x,y).

In order to proceed in the case of a cylinder of arbitrary cross-section ∂D, we must also introduce an appropriate Green function, G, say, for the Helmholtz problem on periodic domains. Such a Green function is generated by a periodic distribution of sources at $(\xi,\eta+2md)$, $-\infty < m < \infty$ incorporating the appropriate phase shift between adjacent sources. Thus

$$(\nabla^2 + k^2)G(x,y|\xi,\eta) = \delta(X)\sum_{m=-\infty}^{\infty}\delta(Y-2md)\mathrm{e}^{\mathrm{i}2m\beta d},$$

where $X = x-\xi$, $Y = y-\eta$ with

$$G(x,y|\xi,\eta) \sim \frac{1}{2\pi}\ln r_m \quad \text{as } kr_m \to 0, \quad r_m^2 = X^2 + (Y-2md)^2, -\infty < m < \infty,$$

and hence, G satisfies the periodicity relations

$$\left.\begin{aligned} G(x,y+2jd|\xi,\eta) &= \mathrm{e}^{\mathrm{i}2\beta jd}G(x,y|\xi,\eta),\\ G(x,y|\xi,\eta-2jd) &= \mathrm{e}^{-\mathrm{i}2\beta jd}G(x,y|\xi,\eta),\end{aligned}\right\} \quad j = -\infty,\ldots,\infty.$$

Alternatively we may write

$$G(x,y|\xi,\eta) = \mathrm{e}^{\mathrm{i}\beta Y}\widehat{G}(x,y|\xi,\eta),$$

where $\widehat{G}$ is a function periodic in both y and η with period $2d$. Referring to the strip $y \in [-d,d]$ the periodicity conditions on $y = \pm d$ are

$$\left.\begin{aligned} G(x,d|\xi,\eta) &= \mathrm{e}^{\mathrm{i}2\beta d}G(x,-d|\xi,\eta), \quad G(x,y|\xi,d) = \mathrm{e}^{-\mathrm{i}2\beta d}G(x,y|\xi,-d),\\ G_\eta(x,d|\xi,\eta) &= \mathrm{e}^{\mathrm{i}2\beta d}G_\eta(x,-d|\xi,\eta), \quad G_\eta(x,y|\xi,d) = \mathrm{e}^{-\mathrm{i}2\beta d}G_\eta(x,y|\xi,-d).\end{aligned}\right\} \tag{2.7}$$

There are many different representations for the Green function on periodic domains to be found in the literature and used in a range of applications. Perhaps the simplest representation for G is the following:

$$G(x,y|\xi,\eta) = -\frac{1}{4}\sum_{m=-\infty}^{\infty}\frac{\mathrm{e}^{-\gamma_m|X|}\mathrm{e}^{\mathrm{i}\beta_m Y}}{\gamma_m d} \tag{2.8}$$

(see, for example, Linton 1998) where

$$\beta_m = \beta + m\pi/d, \quad \gamma_m = (\beta_m^2 - k^2)^{1/2} = -\mathrm{i}(k^2-\beta_m)^{1/2}. \tag{2.9}$$

Note that γ_m are real for all m provided

$$0 < k < \beta < \pi/d - k, \tag{2.10}$$

a condition we impose to ensure that (2.3) is satisfied subsequently. In this case

$$G(x,y|\xi,\eta)\to 0 \quad \text{exponentially as } |X|\to\infty. \tag{2.11}$$

The form of (2.8) is unsuitable for computational purposes as it is slowly convergent for $X=0$ and the singularity as $X,Y\to 0$ is not explicit.

Linton (1998) has compiled a comprehensive list of representations for G, with their derivations and compared their merits in terms of computational efficiency and accuracy. He found that the representation based on Ewald's summation method is best and is given by

$$\begin{aligned} G(x,y|\xi,\eta) = &-\frac{1}{4}\sum_{m=-\infty}^{\infty}\frac{\mathrm{e}^{\mathrm{i}\beta_m Y}}{2\gamma_m d}\left[\mathrm{e}^{\gamma_m X}\mathrm{erfc}\left(\frac{\gamma_m d}{a}+\frac{aX}{2d}\right)+\mathrm{e}^{-\gamma_m X}\mathrm{erfc}\left(\frac{\gamma_m d}{a}-\frac{aX}{2d}\right)\right] \\ &-\frac{1}{4\pi}\sum_{m=-\infty}^{\infty}\mathrm{e}^{\mathrm{i}2\beta m d}\sum_{n=0}^{\infty}\frac{1}{n!}\left(\frac{kd}{a}\right)^{2n}E_{n+1}\left(\frac{a^2r_m^2}{4d^2}\right) \end{aligned} \tag{2.12}$$

(note the change in periodicity from d in Linton's notation to $2d$ here), where E_n is the exponential integral, and a is a positive real, but otherwise arbitrary, parameter which affects the convergence of the two series in (2.12). Linton (1998) notes that increasing a causes the second sum to converge faster and the first slower and vice versa. In the computations we used a value of $a=1$, which appears to be fairly optimal for a range of other parameters.

The frequency $\omega_c=\beta c$ (c is the wave speed) is called the cut-off frequency for the Rayleigh–Bloch problem. Condition (2.10) states that $\omega=kc<\omega_c$, suggesting that we should operate at a frequency below the cut-off frequency. We will assume henceforth that (2.10) is satisfied and, in addition to (2.11), this provides the following properties of G:

$$G(\xi,\eta|x,y)=\bar{G}(x,y|\xi,\eta) \tag{2.13}$$

and

$$G(x,-y|\xi,-\eta)=\bar{G}(x,y|\xi,\eta), \tag{2.14}$$

where the bar denotes complex conjugate. Note that for $\beta d=\frac{1}{2}\pi$, $G(x,y|\xi,\eta)$ is real, a fact which follows from $\beta_m=-\beta_{-m-1}$, $\gamma_m=\gamma_{-m-1}$. Alternatively, it can be argued that G can be chosen to be real without loss of generality since the equations and boundary conditions governing G are all real for this choice of βd.

We will also be concerned with the special value of $\beta d=\pi$, with $k<\beta$, when the Green function is $2d$-periodic. Clearly (2.10) is now violated and $\gamma_{-1}=-\mathrm{i}k$ from (2.9). Thus, from (2.8), $G\sim(-\mathrm{i}/4kd)\mathrm{e}^{\mathrm{i}k|X|}$ as $|X|\to\infty$ and cannot be considered as a valid candidate for constructing Rayleigh–Bloch surface waves. We can, however, define a new Green function for $\beta d=\pi$, which is $2d$-periodic and decays to zero as $|X|\to\pm\infty$. This is the combination

$$G_\pi(x,y|\xi,\eta)=\tfrac{1}{2}\left\{G(x,y|\xi,\eta)-G(x,y|\xi,-\eta)\right\}. \tag{2.15}$$

Then (2.8) is replaced by

$$G_\pi(x,y|\xi,\eta)=-\frac{1}{2}\sum_{m=1}^{\infty}\frac{\mathrm{e}^{-\gamma_{m-1}|X|}}{\gamma_{m-1}d}\sin(m\pi y/d)\sin(m\pi\eta/d),$$

such that, for $k<\beta=\pi/d$, G_π is real and satisfies (2.11), (2.13), (2.14). In addition,

G_π satisfies the Dirichlet conditions

$$G_\pi(x, y|\xi, \eta) = 0, \quad y = 0, \pm d. \tag{2.16}$$

Straightforward substitution of (2.12) into (2.15) gives the Ewald summation Green function representation for G_π that is used in the computations.

3. Formulation of an integral equation and its discretization

In what follows, we label the points (x, y) and (ξ, η) by p and q.

We are now in a position to use Green's Identity to formulate the integral equation. Green's Identity states that

$$\iint_W \Big(\phi(q)\nabla^2 G(p|q) - G(p|q)\nabla^2\phi(q)\Big)\,\mathrm{d}x\,\mathrm{d}y = \int_{\partial W}\left(\phi(q)\frac{\partial G(p|q)}{\partial n_q} - G(p|q)\frac{\partial\phi(q)}{\partial n_q}\right)\mathrm{d}s_q \tag{3.1}$$

for $p \in W$, and n_q denotes the normal with respect to q. Here, W denotes the part of the strip $(-L, L)\times[-d, d]$ occupied by the fluid and ∂W denotes the boundary of W consisting of ∂D (the boundary of the cylinder cross-section) the lines $y = \pm d$, $-L < x < L$ and $x = \pm L$, $-d < y < d$ where $L \to \infty$. Using the periodicity of ϕ, ϕ_y, G and G_η from (2.6), (2.7) and the exponential decay of G from (2.11) reduces (3.1) to

$$\phi(p) = \int_{\partial D}\phi(q)\frac{\partial G(p|q)}{\partial n_q}\,\mathrm{d}s_q, \quad p \notin \partial D, \tag{3.2}$$

whilst

$$\tfrac{1}{2}\phi(p) = \int_{\partial D}\phi(q)\frac{\partial G(p|q)}{\partial n_q}\,\mathrm{d}s_q, \quad p \in \partial D, \tag{3.3}$$

which provides the necessary integral equation for $\phi(p)$ on ∂D. The value of ϕ everywhere in the strip can then be determined from (3.2).

In operator notation, (3.3) is

$$(\mathscr{K}\phi)(p) = \tfrac{1}{2}\phi(p), \quad p \in \partial D, \tag{3.4}$$

where

$$(\mathscr{K}\phi)(p) = \int_{\partial D}\phi(q)\frac{\partial G(p|q)}{\partial n_q}\,\mathrm{d}s_q. \tag{3.5}$$

We also introduce the inner product

$$\langle u, v\rangle = \int_{\partial D} u(p)\bar{v}(p)\,\mathrm{d}s_p.$$

Alternatively, if we formulate the problem by representing the potential as a distribution of sources of strength $\mu(p)$ over ∂D we obtain

$$(\mathscr{K}^*\mu)(p) = \tfrac{1}{2}\mu(p), \quad p \in \partial D,$$

where $\mathscr{K}^*$ is the adjoint of $\mathscr{K}$.

When the cylinder cross-section is symmetric, the integral equation can be simplified by posing it on only one half of ∂D. Replacing y by $-y$ and η by $-\eta$ in (3.3) and using the fact that ∂D is invariant under reflection in $y = 0$ above we can formulate the integral equation as

$$\tfrac{1}{2}\phi(-p) = \int_{\partial D}\phi(-q)\frac{\partial \bar{G}(p|q)}{\partial n_q}\,\mathrm{d}s_q, \quad p \in \partial D, \tag{3.6}$$

where (2.14) has been used. Here, we write $-p$ and $-q$ to represent the points $(x,-y)$ and $(\xi,-\eta)$ respectively. Let $\partial D = \partial D_+ \cup \partial D_-$. Then (3.3) can be written

$$\tfrac{1}{2}\phi(p) = \int_{\partial D_+} \phi(q)\frac{\partial G(p|q)}{\partial n_q}\,\mathrm{d}s_q + \int_{\partial D_+} \psi(q)\frac{\partial H(p|q)}{\partial n_q}\,\mathrm{d}s_q, \quad p \in \partial D_+,$$

where $H(p|q) = G(p|-q)$, $\psi(p) = \phi(-q)$ and (3.6) is

$$\tfrac{1}{2}\psi(p) = \int_{\partial D_+} \phi(q)\frac{\partial \bar{H}(p|q)}{\partial n_q}\,\mathrm{d}s_q + \int_{\partial D_+} \psi(q)\frac{\partial \bar{G}(p|q)}{\partial n_q}\,\mathrm{d}s_q, \quad p \in \partial D_+,$$

and (2.13) and (2.14) have been used in the above pair of equations. More compactly, these coupled integral equations can be written in operator notation as

$$\left.\begin{aligned}(\mathscr{G}\phi)(p) + (\mathscr{H}\psi)(p) &= \tfrac{1}{2}\phi(p),\\ (\bar{\mathscr{H}}\phi)(p) + (\bar{\mathscr{G}}\psi)(p) &= \tfrac{1}{2}\psi(p),\end{aligned}\right\} \quad p \in \partial D_+, \tag{3.7}$$

where

$$(\mathscr{G}\phi)(p) = \int_{\partial D_+} \phi(q)\frac{\partial G(p|q)}{\partial n_q}\,\mathrm{d}s_q, \quad (\mathscr{H}\phi)(p) = \int_{\partial D_+} \phi(q)\frac{\partial H(p|q)}{\partial n_q}\,\mathrm{d}s_q.$$

It follows from (3.7) that

$$\phi(p) = c\bar{\phi}(-p), \quad |c| = 1.$$

In fact we can arrive at this result from the governing equations using physical arguments. Assume, therefore, that $\phi(x,y)$ is a solution to (2.1), (2.2) and (2.3). Then $\bar{\phi}(x,y)$ must also be a solution and from (2.5) satisfies

$$\bar{\phi}(x,y) = \mathrm{e}^{-\mathrm{i}\beta y}\overline{\widehat{\phi}(x,y)}.$$

Physically, the potential $\bar{\phi}$ represents a wave travelling in the opposite direction along the array. Since the geometry is symmetric about the line $y = 0$, $\phi(x,y)$ must be related to $\bar{\phi}(x,-y)$ by a constant, c say. In other words

$$\phi(x,y) = c\bar{\phi}(x,-y),$$

and by replacing y by $-y$, it is easily seen that $|c| = 1$. Writing c as $\mathrm{e}^{-2\mathrm{i}\alpha}$ we have

$$\phi(x,y) = \mathrm{e}^{-2\mathrm{i}\alpha}\bar{\phi}(x,-y), \tag{3.8}$$

and the phase α is fixed by taking $y = 0$ in the above, though it remains an unknown of the problem.

Solution

The condition for the existence of a Rayleigh–Bloch surface wave is that (3.3) is satisfied with $\phi(p) \not\equiv 0$ for a real value of k. In order to numerically compute these values of k, we follow Linton & Evans (1992), letting ∂D be given in the polar coordinates by $(\rho(\theta),\theta)$ and parametrizing the points p and q by θ and χ respectively. Then

$$\tfrac{1}{2}\phi(\theta) = \int_0^{2\pi} \phi(\chi)\frac{\partial G(\theta|\chi)}{\partial n_q}w(\chi)\,\mathrm{d}\chi, \quad 0 \leqslant \theta < 2\pi, \tag{3.9}$$

where $w(\theta) = \{\rho^2(\theta) + \rho'^2(\theta)\}^{1/2}$ and

$$\frac{\partial}{\partial n_q} = \frac{1}{w(\chi)}\left(x'(\chi)\frac{\partial}{\partial \eta} - y'(\chi)\frac{\partial}{\partial \xi}\right).$$

We use the Green function representation in (2.12), which is well-behaved everywhere apart from at $kr_0 \to 0$ where G has a logarithmic singularity. In this case, where $p = q$, we write $G = \tilde{G} + \log(r_0)/2\pi$ and take the limit $r_0 \to 0$, where

$$\tilde{G}(p|q) = -\frac{1}{4}\sum_{m=-\infty}^{\infty}\frac{e^{i\beta_m Y}}{2\gamma_m d}\left[e^{\gamma_m X}\operatorname{erfc}\left(\frac{\gamma_m d}{a}+\frac{aX}{2d}\right)+e^{-\gamma_m X}\operatorname{erfc}\left(\frac{\gamma_m d}{a}-\frac{aX}{2d}\right)\right]$$
$$-\frac{1}{4\pi}\sum_{\substack{m=-\infty\\ \neq 0}}^{\infty}e^{i2\beta m d}\sum_{n=0}^{\infty}\frac{1}{n!}\left(\frac{kd}{a}\right)^{2n}E_{n+1}\left(\frac{a^2r_m^2}{4d^2}\right)-\frac{1}{4\pi}\sum_{n=2}^{\infty}\frac{1}{n!}\left(\frac{kd}{a}\right)^{2n}E_{n+1}(0)$$

since in (2.12), the logarithmic singularity is embedded in the exponential integral $E_1(a^2r_0^2/4d^2)$, whilst

$$\lim_{r_0\to 0}\frac{\partial}{\partial n_q}\left(\frac{1}{2\pi}\log r_0\right)=\frac{1}{4\pi w^3(\chi)}\{\rho'(\chi)\rho''(\chi)-\rho^2(\chi)-2\rho'^2(\chi)\}$$

(see Linton & Evans (1992) for more details).

We discretize the interval $[0, 2\pi]$ in (3.9) into $2M$ equal segments of length π/M and collocate at $\theta_i = (i - \frac{1}{2})\pi/M$, $i = 1, \ldots, 2M$ to arrive at the system

$$\tfrac{1}{2}\phi(\theta_i) = \frac{\pi}{M}\sum_{j=1}^{2M}K_{ij}\phi(\theta_j), \quad i = 1, \ldots, 2M,$$

where

$$K_{ij} = w(\theta_i)\frac{\partial G(\theta_i|\theta_j)}{\partial n_q},$$

treating carefully the special case $i = j$ in the manner described above. Rayleigh–Bloch waves correspond numerically to the vanishing of the $2M \times 2M$ complex determinant with elements

$$\delta_{ij} - \frac{2\pi}{M}K_{ij}. \tag{3.10}$$

The difficulty here lies in the fact that we are restricted to using real values of k to seek zeros of a generally complex determinant.

If the cylinder cross-section is symmetric, the symmetries in the coupled system (3.7) allow a simplification to the computational requirements. In this case, we follow the discretizing procedure outlined above, but since the coupled system is only defined on ∂D_+, the positive half of ∂D, we only need to collocate at $\theta_i = (i - \frac{1}{2})\pi/M$, $i = 1, \ldots, M$. The final system is

$$\left.\begin{aligned}\frac{\pi}{M}\sum_{j=1}^{M}\{G_{ij}\phi(\theta_j)+H_{ij}\psi(\theta_j)\} &= \tfrac{1}{2}\phi(\theta_i),\\ \frac{\pi}{M}\sum_{j=1}^{M}\{\bar{H}_{ij}\phi(\theta_j)+\bar{G}_{ij}\psi(\theta_j)\} &= \tfrac{1}{2}\psi(\theta_i),\end{aligned}\right\} \quad i = 1, \ldots, M,$$

and then Rayleigh–Bloch surface waves correspond to the vanishing of the $2M \times 2M$ complex determinant of the matrix

$$\frac{2\pi}{M}\boldsymbol{K} - \boldsymbol{I} \tag{3.11}$$

where $\boldsymbol{K} = \{K_{ij}\}$, $\boldsymbol{I} = \{\delta_{ij}\}$, $i, j = 1, \ldots, 2M$, and we have defined the block-matrix

$$\boldsymbol{K} = \begin{pmatrix} \boldsymbol{G} & \boldsymbol{H} \\ \overline{\boldsymbol{H}} & \overline{\boldsymbol{G}} \end{pmatrix}$$

with $\boldsymbol{G} = \{G_{ij}\}$, $\boldsymbol{H} = \{H_{ij}\}$, $i, j = 1, \ldots, M$,

$$G_{ij} = w(\theta_i)\frac{\partial G(\theta_i|\theta_j)}{\partial n_q}, \quad H_{ij} = w(\theta_i)\frac{\partial G(\theta_i| - \theta_j)}{\partial n_q}.$$

Although the matrix $\boldsymbol{K}$ is complex, the determinant of (3.11) is in fact real. This is as a consequence of the block structure of $\boldsymbol{K}$ and can be shown as follows. First define the unitary matrix $\boldsymbol{U} = \{\delta_{i,2M+1-i}\}$, $i = 1, \ldots, 2M$, having zero entries everywhere apart from values of 1 along the 'wrong' diagonal. Then, since $\det\{\boldsymbol{U}\} = 1$ and $\boldsymbol{U}^2 = \boldsymbol{I}$,

$$\det\left\{\frac{2\pi}{M}\boldsymbol{K} - \boldsymbol{I}\right\} = \det\left\{\frac{2\pi}{M}\boldsymbol{U}\boldsymbol{K}\boldsymbol{U} - \boldsymbol{U}^2\right\} = \det\left\{\frac{2\pi}{M}\overline{\boldsymbol{K}} - \boldsymbol{I}\right\} = \overline{\det\left\{\frac{2\pi}{M}\boldsymbol{K} - \boldsymbol{I}\right\}}$$

and hence the determinant is real.

There is a second instance under which the generally complex determinant system can be reduced to a real one: when the Green function itself is purely real. This occurs when βd takes the specific values $\frac{1}{2}\pi$ and π (see the discussion at the end of § 2), although since we use G_π in (2.15) for $\beta d = \pi$, this has the effect of imposing Dirichlet conditions $\phi(x, y) = 0$ on $y = 0, \pm d$. This antisymmetry about the line $y = 0$ implies that the use of G_π is only valid for cylinders whose cross-sections are symmetric. No such restriction applies when $\beta d = \frac{1}{2}\pi$.

The numerical procedure

Let us first discuss the numerical procedure, which is common to all results that follow. In every case below, we are concerned with finding real values of kd for which the determinant of the system having elements given by (3.10) vanishes. The computation of the elements K_{ij} requires the evaluation of derivatives of the Green function, G. We use the representation for G given by (2.12), whose explicit derivatives with respect to ξ and η can be computed very accurately and efficiently (this is not always the case with other representations of G!). We use a value of $a = 1$ for the arbitrary parameter which suffices for our purpose, though it could no doubt be optimized (see Linton 1998). The remaining parameter in the numerical procedure is M, which controls the number of collocation points used. For most cylinder cross-sections with 'smooth' boundaries, the choice $M = 16$ ensures that the determinant is accurate to at least four decimal places. There are cases when the numerical method may break down, for example if the width of the cross-section is greater than about 90% of the period (since there is interference with the image of Green functions as adjacent cylinders in the array become too close). Inaccuracies can also creep into the computations if the ratio of width to length of the cross-section becomes too small (below one in four) since then there is interference between close source points on opposite sides of the cylinder. It should be emphasized that this is a manifestation of the approximation scheme we have employed and has nothing to do with the validity of the integral equations themselves. For cylinder cross-sections with non-smooth boundaries, such as rectangles, the value of M has to be increased to retain the four decimal place accuracy. A more sophisticated numerical scheme should be used for cross-sections with such boundaries, but for our purposes the one used here is sufficient.

Throughout the results section we will concentrate on cylinder cross-sections of the

a/d	$M = 8$	$M = 16$	Evans & Porter (1998)
0.2	1.49692	1.49698	1.49699
0.4	1.43001	1.49010	1.49012
0.6	1.33974	1.33985	1.33987
0.8	1.31273	1.31306	1.31309
1.0	1.42786	1.41129	1.41205

TABLE 1. The convergence of the numerical scheme for a circular cylinder radius a with $\beta d = 1.5$.

form

$$(x_\theta/a)^n + (y_\theta/b)^n = 1, \tag{3.12}$$

where

$$x_\theta = x\cos\theta - y\sin\theta, \quad y_\theta = x\sin\theta + y\cos\theta$$

are coordinates rotated through an angle θ. Such a cross-section provides many possibilities. For example, when $n = 2$, we have an ellipse of aspect ratio b/a. As $n \to \infty$ we recover a rectangular cross-section of length $2a$ and width $2b$ and for $n = 1$ we have a parallelogram of diagonal lengths $2a$ and $2b$. Finally, all these symmetric cross-sections can be made unsymmetric by rotating through an angle θ.

The numerical method has been checked against existing results for Rayleigh–Bloch surface waves in the cases of circular and rectangular cross-sections (see Evans & Porter 1998 and Evans & Fernyhough 1995 respectively). Table 1 shows the convergence of values of kd with M in the case of a circular cylinder and compares them with the accurate results of Evans & Porter (1998).

4. Results for symmetric cross-sections

4.1. *Rayleigh–Bloch solutions for symmetric cross-sections*

In this section results are presented for cylinder cross-sections which are symmetric with respect to the plane perpendicular to the plane containing the cylinders in the array. We recall from the previous section that, in this symmetric configuration, the Rayleigh–Bloch surface waves correspond to the vanishing of a real determinant for some real wavenumber, kd.

A typical set of results for Rayleigh–Bloch surface waves is shown in figure 1. These show the variation of kd with βd for a range of symmetric elliptical cross-sections of length $a/d = 1$ and aspect ratios of $b/a = \frac{3}{4}$, $\frac{1}{2}$ and $\frac{1}{4}$. Also shown in figure 1 is the Rayleigh–Bloch dispersion curve for an infinite periodic array of thin parallel plates of length $a/d = 1$ computed using the approximate formula of Evans & Linton (1993). Thus for a particular choice of Rayleigh–Bloch wavenumber βd, periodicity of $2d$ and plate length $2a$, values of $k < \beta$ satisfy

$$ka - \tfrac{1}{2}\pi = \sum_{n=1}^{\infty}\left\{\sin^{-1}\left(\frac{2kd}{n\pi}\right) - \sin^{-1}\left(\frac{k}{\beta_n}\right) - \sin^{-1}\left(\frac{k}{|\beta_{-n}|}\right)\right\} + \frac{2kd}{\pi}\ln 2 - \sin^{-1}\left(\frac{k}{\beta}\right).$$

It is interesting to note how the Rayleigh–Bloch results converge to those for a flat plate as the ellipse is made thinner. In fact the agreement between the results for a plate and an ellipse of aspect ratio of $b/a = \frac{1}{4}$ is to within just over 1%.

Notice from figure 1 that we only consider $0 < \beta d \leqslant \frac{1}{2}\pi$. This is due to the fact

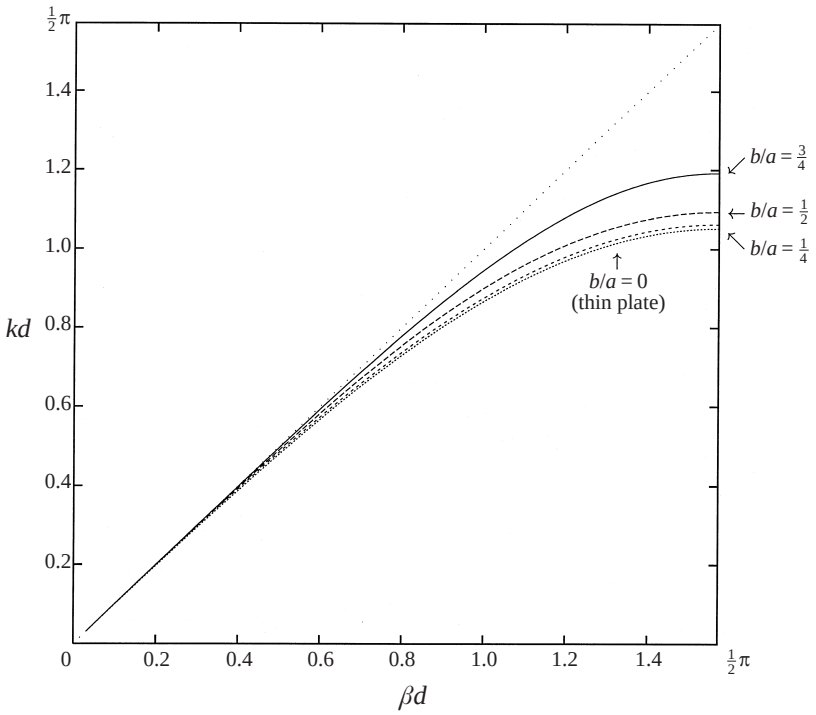

FIGURE 1. The variation of kd with βd for elliptical cross-sections $(x/a)^2 + (y/b)^2 = 1$, $a/d = 1$ with various aspect ratios b/a shown against curves. Also shown are the 'approximate' results for a thin flat plate.

that

$$kd(\beta d) = kd(\pi - \beta d), \quad \text{and} \quad kd(\beta d) = kd(j\pi + \beta d), \quad j = 1, \ldots . \tag{4.1}$$

The latter of these is obvious from inspection of (2.8), (2.9), whilst the former can be shown simply by letting $\beta' d = \pi - \beta d$ and then from (2.9), $\beta'_m = -\beta_{-m-1}$ and $\gamma'_m = \gamma_{-m-1}$. Using this in (2.8), for example, with primes indicating the use of β' shows that

$$G'(x, y|\xi, \eta) = \bar{G}(x, y|\xi, \eta).$$

Also, from (2.4), $\phi'(x, y + 2jd) = \mathrm{e}^{-\mathrm{i}2\beta' dj}\phi'(x, y)$ so that

$$\phi'(x, y) = \bar{\phi}(x, y).$$

It follows from using Green's Identity in (3.1) with ϕ' and G' replacing ϕ and G that

$$\tfrac{1}{2}\phi'(p) = \int_{\partial D} \phi'(q) \frac{\partial G'(p|q)}{\partial n_q} \, \mathrm{d}s_q$$

and conjugating this results in the integral equation (3.3).

Rayleigh–Bloch results can also be computed for $\beta d = \pi$, when G_π defined in (2.15) is used. Thus, for the three values of $b/a = \frac{1}{4}, \frac{1}{2}, \frac{3}{4}$, the corresponding values of $kd(\pi)$ are 2.93966, 2.96010, 2.83631 respectively.

A different way of representing the results is presented in figure 2, where curves of kd against b/d are plotted for various values of βd in the case of an elliptical cross-section of constant aspect ratio $b/a = \frac{1}{2}$ so that b/d measures the size of the cylinder.

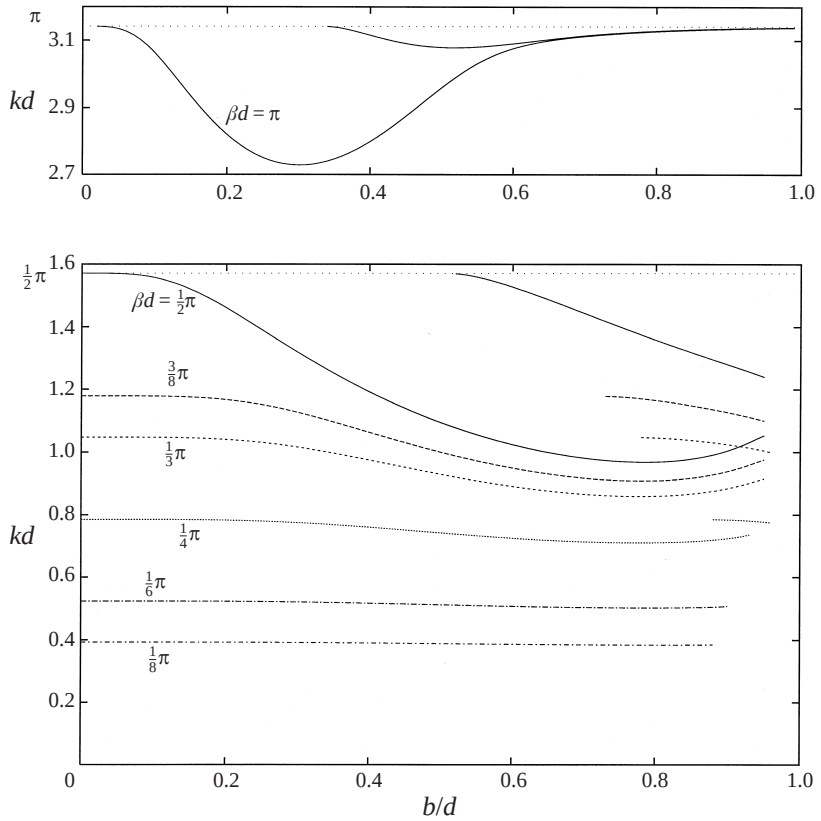

FIGURE 2. Curves of wavenumber, kd, versus geometry b/d for elliptical cylinders with constant aspect ratio $b/a = \frac{1}{2}$ and for various values of βd shown against curves.

The results stop short of $b/d = 1$ due to numerical difficulties. Notice that, for each value of βd shown, there is a Rayleigh–Bloch mode which exists for all $0 < b/d \leqslant 1$, and, for b/d large enough, a second mode appears. This is just the next highest mode which is capable of being supported due to the increased length of the cylinder and is antisymmetric about the line joining the cylinders in the array. For longer cylinders further modes occur alternating between symmetric and antisymmetric about this line joining the cylinders (see, for example, Evans & Linton 1993). Notice that the extra graph for $\beta d = \pi$ required the use of G_π. The particular values of βd chosen in figure 2 are of relevance to the following subsection.

The results shown in figures 1 and 2 are typical of Rayleigh–Bloch solutions for many other cylinder cross-sections.

4.2. *Trapped modes about multiple cylinders spanning a channel or waveguide*

We have seen that for a each infinite array of symmetric cylinder cross-sections it is possible, for each choice of $\beta d \leqslant \frac{1}{2}\pi$, to find value(s) of kd corresponding to Rayleigh–Bloch surface waves. However, by choosing appropriate forms for βd we can enforce certain periodic conditions on the solutions which can be interpreted as describing trapped modes at that wavenumber kd in a waveguide or channel spanned by any (finite) number of cylinders of identical cross-section. This observation was also noted in McIver *et al.* (1998) who considered Rayleigh–Bloch surface waves along coastlines generated by periodic arrays that were generated by singular potentials.

Assume that each cylinder cross-section, D, is symmetric as in the previous section. First we redefine the location of the origin, and place it for convenience to coincide with a line of geometric symmetry between two adjacent cylinders. Then $y = 2Nd$ is also a line of geometric symmetry bisecting the Nth and $(N+1)$th cylinders. The strip of width $2Nd$ now contains N cylinders.

Recall from (2.4) the relation

$$\phi(x, y + 2Nd) = \mathrm{e}^{\mathrm{i}2N\beta d}\phi(x, y),$$

the same periodicity relation also being satisfied by the function $\phi_y(x, y)$. Thus we can ensure the solution is periodic in y with period $2Nd$ by choosing

$$\beta d = n\pi/N, \quad n = 1, \ldots, N. \tag{4.2}$$

In fact, since $kd(\beta d) = kd(\pi - \beta d)$ from (4.1), only the values of $n = 1, \ldots, [\frac{1}{2}N]; N$, where $[x]$ denotes the integer part of x, are needed to construct the complete set of values of kd.

Alternatively, a 'half-periodic' potential can be constructed by choosing

$$\beta d = (n - \tfrac{1}{2})\pi/N, \quad n = 1, \ldots, [\tfrac{1}{2}(N+1)], \tag{4.3}$$

such that $\phi(x, y + 2Nd) = -\phi(x, y)$ and $\phi_y(x, y + 2Nd) = -\phi_y(x, y)$. That is, the potential has opposite signs in adjacent $2Nd$-width strips. In general, therefore, $\beta d = m\pi/2N$, $m = 1, \ldots, N$; $2N$ gives rise to either $2Nd$-periodic (m even) or $2Nd$-half-periodic (m odd) functions $\phi(x, y)$. There are, then, for N cylinders, a total of $N + 1$ values of βd leading to $N + 1$ distinct values of kd.

Since we have chosen $y = 0$ to coincide with a line of geometric symmetry we can apply the relation in (3.8) and may, without loss of generality, incorporate an arbitrary phase into the potential ϕ. Thus, we consider the potential

$$\chi(x, y) = \mathrm{e}^{\mathrm{i}\alpha}\phi(x, y)$$

whence

$$\chi(x, y) = \bar{\chi}(x, -y).$$

Now since $\chi(x, y)$ is a Rayleigh–Bloch solution, then its symmetric and antisymmetric parts, decomposed about the line of geometric symmetry, also satisfy all the conditions of the problem. We can therefore consider the following two potentials:

$$\chi^N(x, y) = \mathrm{Re}\,\{\chi(x, y)\}, \quad \chi^D(x, y) = \mathrm{Im}\,\{\chi(x, y)\}$$

such that

$$\chi^N(x, y) = \chi^N(x, -y) \quad \text{and} \quad \chi^D(x, y) = -\chi^D(x, -y),$$

and as a consequence,

$$\chi^N_y(x, 0) = 0 \quad \text{and} \quad \chi^D(x, 0) = 0,$$

where it is now clear that the superscripts N and D indicate that the potentials satisfy Neumann and Dirichlet (respectively) conditions on the line $y = 0$. Note that these two potentials are purely real, a property which is typical of standing waves since with time re-introduced into the full potential we have

$$\Phi^{N,D}(x, y, z, t) = \chi^{N,D}(x, y)\cosh k(H - z)\cos \omega t.$$

There are now four different situations available to us. These are best represented schematically by a typical cross-section of the $2Nd$-width strip as in figure 3. Let us

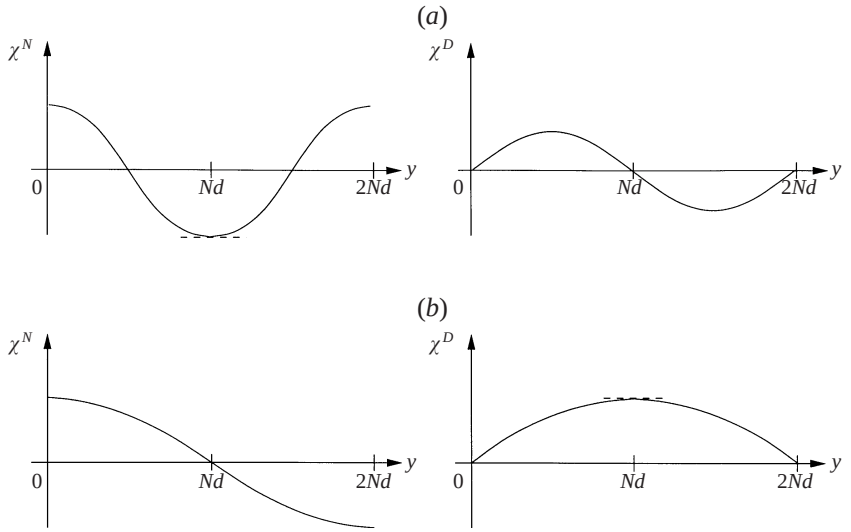

FIGURE 3. The features of the four possible modes corresponding to (*a*) periodic and (*b*) half-periodic solutions in a uniform strip of width $2Nd$ containing N cylinders.

justify the form of the possible potentials in this figure. Clearly, when the solution is periodic $\chi^{N,D}(x,0) = \chi^{N,D}(x,2Nd)$ and $\chi^{N,D}_y(x,0) = \chi^{N,D}_y(x,2Nd)$ which fixes the behaviour at the two extremes of the strip in figure 3(*a*). Within each strip, the cylinders are arranged symmetrically about the centre of the strip which allows both χ^N and χ^D to be decomposed further into their symmetric and antisymmetric parts. In each case, however, one of these must be identically zero because otherwise it would contradict the behaviour already established at the ends of the strip. Thus, for a periodic solution, χ^N must also be an even function in y across $y = Nd$ (the centre of the strip). Similarly, for a periodic solution, χ^D must be odd in y across $y = Nd$.

For half-periodic solutions, similar arguments apply. The functions $\chi^{N,D}$ and their derivatives take opposite values at the two extremes of the strip, which fixes their behaviour at $y = 0,\ 2Nd$. Again, geometric symmetry about the centre of the strip allows further decomposition into symmetric and antisymmetric components, only one of which is not identically zero in each of the Neumann and Dirichlet cases. The functions χ^N and χ^D must therefore take the form shown in figure 3(*b*), with χ^N odd about $y = Nd$ and χ^D even.

Note that figure 3 only demonstrates the general features of the profile in y across the strip. Within these restrictions, the functions $\chi^{N,D}$ may take on a general form and do, of course, vary with x.

We consider first the case of $N = 1$ when $\beta d = \frac{1}{2}\pi,\ \pi$ correspond to half-periodic and periodic solutions respectively in a strip of width $2d$ containing a single cylinder symmetric about $y = d$, and the possible solutions are again described by figures 3(*a*), 3(*b*) but with $N = 1$. The possibility of a solution χ^D with $\beta d = \frac{1}{2}\pi$ as in figure 3(*b*) having Dirichlet conditions on $y = 0,\ 2d$, is ruled out by a theorem of McIver & Linton (1995, p. 548, equation (3.7)) which shows that no trapped modes exist with $kd < \frac{1}{2}\pi$ provided that the upper half of the cylinder can be described by a function $f : x \to f(x)$. The solution χ^N with $\beta d = \frac{1}{2}\pi$ described in figure 3(*b*) is just the well-known antisymmetric Neumann trapped mode about a symmetric cylinder on the centreline of a channel, the existence of which was proved by Evans *et al.* (1994).

For $\beta d = \pi$, the Green function G_π defined by (2.15) is used and so (2.16) implies that the solution must correspond to χ^D as shown in figure 3(*a*). This corresponds to an antisymmetric trapped mode about a single cylinder placed on the centreline of a channel having Dirichlet conditions on the walls. This Dirichlet trapped mode does not always exist. However, the method used by Evans *et al.* (1994) to show the existence of trapped modes in a Neumann waveguide can easily be adapted to consider the case of a waveguide having Dirichlet conditions on the walls containing a cross-section described by $f: x \to f(x)$, $-a < x < a$, with $f(\pm a) = 0$ to show that a Dirichlet trapped mode exists provided

$$\int_{-1}^{1} \sin(2\pi f(ax)/d)\,\mathrm{d}x > 0. \tag{4.4}$$

Note that this inequality is independent of the length of the cylinder in the waveguide. In the case of a circular cylinder, for example, (4.4) reduces to $J_1(2\pi a/d) > 0$ or $a/d \lesssim 0.61$, consistent with the result $a/d \lesssim 0.68$ of Maniar & Newman (1997). It is evident from (4.4) that a Dirichlet trapped mode exists for all cylinder sections occupying not more than half the channel width. Using cylinder cross-sections given by (3.12), we can use (4.4) to shed some light on what other features of the geometry dictate the existence of trapped modes in Dirichlet waveguides. Thus, in figure 4, the solid curve represents the maximum width, b/d, of a cross-section $(x/a)^n + (y/b)^n = 1$, below which existence of a Dirichlet trapped mode is guaranteed *for all lengths of cylinder cross-section* a/d. Also shown in figure 4 are computed curves of the actual range of existence of Dirichlet trapped modes for particular values of a/d. As $n \to \infty$, the results converge to $b/d = \frac{1}{2}$ in agreement with the specific analysis for a rectangular block which reveals that Dirichlet trapped modes do not exist for $b/d > \frac{1}{2}$. As $a/d \to 0$, corresponding to a narrowing cylinder, the results converge to the theoretical curve computed from (4.4) indicating that the inequality (4.4) which is independent of a/d is sharp. As a/d increases, the range of values of b/d increases for a particular value of n.

Returning to general N, we have seen that there are, in general, for N cylinders in a channel of width $2Nd$, $N+1$ possible values of βd given by $\beta d = m\pi/2N$, $m = 1, \ldots, N; 2N$ giving rise to trapped modes. The condition (2.4) shows that the particular values $\beta d = \frac{1}{2}\pi$, π give rise to solutions which are half-periodic or periodic respectively, in each of the sub-channels of width $2d$ containing a single cylinder. These solutions are just the Neumann mode, and the Dirichlet mode, where it exists, respectively discussed above in the case $N = 1$. Thus the solution in the full channel of width $2Nd$ in this case is simply the superposition of the Neumann or Dirichlet mode for a single cylinder in each of the sub-channels of width $2d$.

For the remaining $N-1$ values of βd, ϕ is complex and both χ^N and χ^D give rise to possible solutions for the same value of kd, having the general structure described in figure 3. Of particular interest is the conclusion that, for $N > 1$, those χ^N described by figure 3(*a*) also satisfy a Neumann condition on the centreline of the channel of width $2Nd$ spanned by N cylinders. For N even this is not surprising since the solution is then simply equivalent to two channels, each of width Nd with trapped modes which are mirror images of each other. But for N odd, the centreline of the channel is occupied by a cylinder and there are $\frac{1}{2}(N-1)$ identical cylinders equally-spaced either side of it. Thus, whereas a single cylinder on the centreline of a channel requires the solution of a Neumann trapped mode to be odd about the centreline as in Evans *et al.* (1994), the introduction of additional pairs of cylinders either side of the centreline

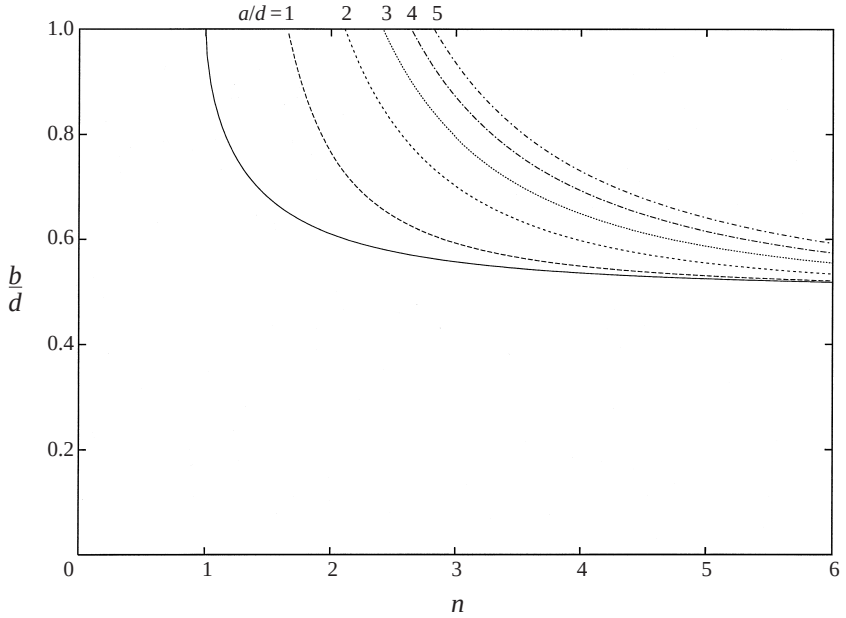

FIGURE 4. Curves showing maximum width, b/d, of a cylinder in a Dirichlet waveguide for which trapped modes exist for a cylinder cross-section $(x/a)^n + (y/b)^n = 1$ as n varies. Values of a/d are shown above curves. The solid curve shows maximum cylinder width predicted from equation (4.5).

results in two different types of Neumann trapped modes, χ^N, which can be either odd or even about the centreline.

A similar conclusion can be deduced about χ^D, for $N > 1$, where both types described in figure 5(a, b) arise, in contrast to the single cylinder case where only the Dirichlet mode described by χ^D in figure 5(a) occurs.

Thus, for a configuration of N cylinders, there is a total of N Neumann trapped modes and up to N Dirichlet trapped modes.

An example of the trapped mode wavenumbers that occur for $N = 1, \ldots, 5$ circular cylinders each of radius $a/d = \frac{1}{2}$ placed periodically across a waveguide of width $2Nd$ is shown in table 2. For each value of N, the set of $N+1$ values of βd is given by (4.2) and (4.3) and Rayleigh–Bloch theory is then used to calculate the values of $kd(\beta d)$. The importance of the curves in figures 1 and 2 is now evident. For a particular symmetric cross-section, there exists a curve of βd against kd, from which trapped mode wavenumbers for N cylinders in a waveguide are given simply by reading off kd at values of $\beta d = m\pi/2N$, $m = 1, \ldots, N; 2N$. Alternatively, for a fixed number of cylinders in a waveguide, curves such as those shown in figure 2 for appropriate values of βd give the trapped mode wavenumbers, kd, over a range of cross-sections.

The first two columns in table 2 correspond to Dirichlet and Neumann modes about each of the cylinders separately so that the problem has degenerated into the motion in N separate sub-channels each of width $2d$. Note that the trapped mode wavenumbers $kd(\beta d)$ for $N > 1$ lie within the continuous spectra $[\pi/2Nd, \infty)$ and $[\pi/Nd, \infty)$ for Neumann and Dirichlet waveguides respectively of width $2Nd$. Other values of βd give rise to both Neumann and Dirichlet modes at the same value of kd. Note that for $N > 1$, all but the smallest value of kd is above the lowest point of the continuous spectrum for a channel of width $2Nd$. The values of kd in table 2 are in exact agreement with those of Utsunomiya & Eatock Taylor (1998).

N	Dirichlet only	Neumann only	Dirichlet and Neumann			
	(π)	$(\frac{1}{2}\pi)$				
1	3.07172	1.39131				
	(π)	$(\frac{1}{2}\pi)$	$(\frac{1}{4}\pi)$			
2	3.07172	1.39131	0.78027			
	(π)	$(\frac{1}{2}\pi)$	$(\frac{1}{3}\pi)$	$(\frac{1}{6}\pi)$		
3	3.07172	1.39131	1.03184	0.52227		
	(π)	$(\frac{1}{2}\pi)$	$(\frac{3}{8}\pi)$	$(\frac{1}{4}\pi)$	$(\frac{1}{8}\pi)$	
4	3.07172	1.39131	1.15193	0.78027	0.392164	
	(π)	$(\frac{1}{2}\pi)$	$(\frac{2}{5}\pi)$	$(\frac{3}{10}\pi)$	$(\frac{1}{5}\pi)$	$(\frac{1}{10}\pi)$
5	3.07172	1.39131	1.22016	0.93245	0.62592	0.31389

TABLE 2. Trapped mode wavenumbers $kd(\beta d)$ (values of βd shown in brackets above) for N circular cross-sections, $a/d = \frac{1}{2}$, in a parallel waveguide with either Dirichlet or Neumann conditions placed upon the walls.

By way of a demonstration of the form that these trapped modes take in a channel, we look at the surface elevation for all the possible modes that occur for $N = 3$ elliptical cylinders of dimensions $a/d = 1$, $b/a = \frac{1}{2}$. Then from (4.2) and (4.3) the relevant Rayleigh–Bloch wavenumbers are just $\beta d = \{\pi, \frac{1}{2}\pi, \frac{1}{3}\pi, \frac{1}{6}\pi\}$. The corresponding values of kd can be read off from figure 2 with $b/d = \frac{1}{2}$ and computations show that the values are $\{2.96010, 1.09407, 0.92982, 0.51252\}$. Of course, for $\beta d = \pi$ the trapped mode is effectively just three parallel Dirichlet-walled channels placed side by side. The same is true for $\beta d = \frac{1}{2}\pi$, only with Neumann wall conditions. The surface elevations of these two modes are shown, for a single cylinder, in figures 5(a) and 5(b). The shading on the inside of the cylinder refers to the level $\phi = 0$, whilst light/dark shading represents peaks/troughs. Since the trapped mode corresponds to a homogeneous solution, the surface elevation may be scaled by an arbitrary factor. For extra information, the straight lines on which Neumann and Dirichlet conditions apply are denoted in the figures by N and D respectively. It is apparent that the field close to the cylinder surface is not represented very accurately. This is due to the fact that the field outside the cylinder is calculated numerically using the discrete form of (3.2) which replaces the continuous distribution of sources around the cylinder with a discrete distribution. Instead, the field in the vicinity of the cylinder has been calculated by crudely extrapolating the value of ϕ on ∂D into the field so as to satisfy (2.2). The value of ϕ on ∂D is computed at the discrete points $\phi(\theta_i)$ which represent the components of the eigenvector, Φ, corresponding to the eigenvalue $\lambda = 0$ in the system $((2\pi/M)\boldsymbol{K} - \boldsymbol{I})\Phi = \lambda\Phi$.

For $\beta d = \frac{1}{3}\pi$ or $\frac{1}{6}\pi$, the situation is more complicated. Here, for each value of βd both Neumann (χ^N) and Dirichlet (χ^D) modes exist at the same value of kd, but take independent modal shapes. Thus, for $\beta d = \frac{1}{3}\pi$, the lower-right-hand quadrant of the field for the function χ^N is shown in figure 6(a) having Neumann conditions on the channel walls and on the centreline in contrast to the single cylinder case, whilst χ^D is shown in figure 6(b) with Dirichlet conditions on both the walls and the centreline. These are in agreement with the features demonstrated in figure 3(a). In order to restore the full waveguide, one must make appropriate reflections about the two centrelines. Similarly, for $\beta d = \frac{1}{6}\pi$, corresponding to a half-periodic solution we

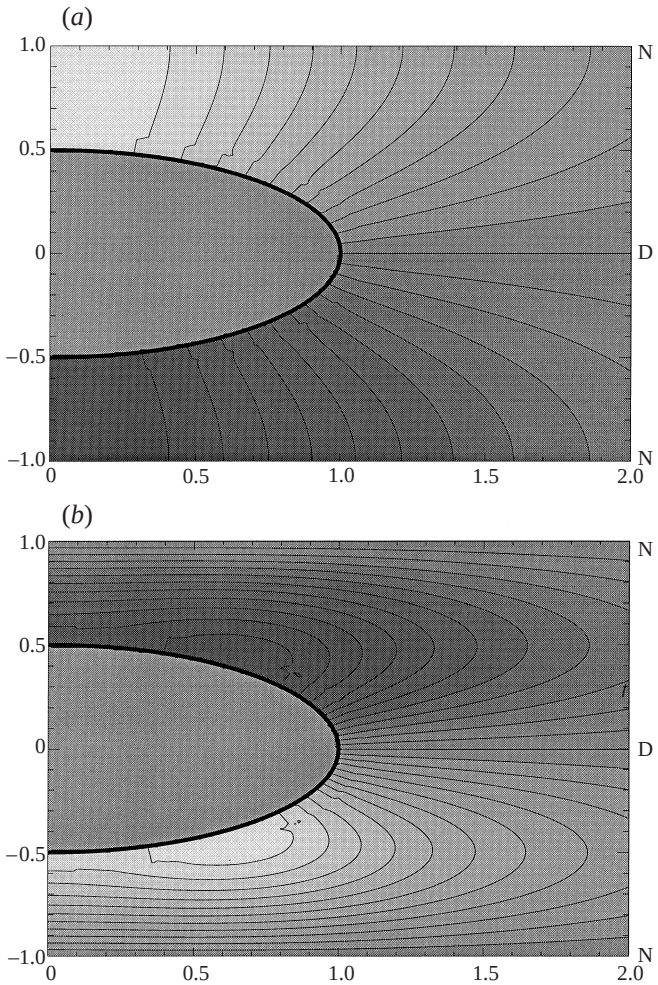

FIGURE 5. The field for (*a*) the Neumann ($\beta d = \frac{1}{2}\pi$) and (*b*) Dirichlet ($\beta d = \pi$) trapped modes about a elliptical cylinder, $b/a = \frac{1}{2}$.

expect the modal form in figure 3(*b*). This is confirmed in the surface elevation plots of figures 7(*a*) and 7(*b*) for the two functions χ^N and χ^D.

It is now easy to visualize the trapped modes for other numbers of cylinders spanning a channel. For example, with $N = 4$ cylinders, we expect five different situations: two modes consist of four single-cylinder Dirichlet trapped modes placed side by side ($\beta d = \pi$), and four Neumann trapped modes placed side by side ($\beta d = \frac{1}{2}\pi$); another is formed by gluing together two trapped modes corresponding to two cylinders in a channel ($\beta d = \frac{1}{4}\pi$); and two more exist for the full four cylinders ($\beta d = \frac{3}{8}\pi$, $\frac{1}{8}\pi$).

5. Results for unsymmetric cross-sections with $\beta d = \frac{1}{2}\pi$

We have already noted in § 3 how the generally complex determinant leading to Rayleigh–Bloch mode wavenumbers can be made real by choosing the specific value of $\beta d = \frac{1}{2}\pi$, without having made any restrictions on the choice of geometry. In

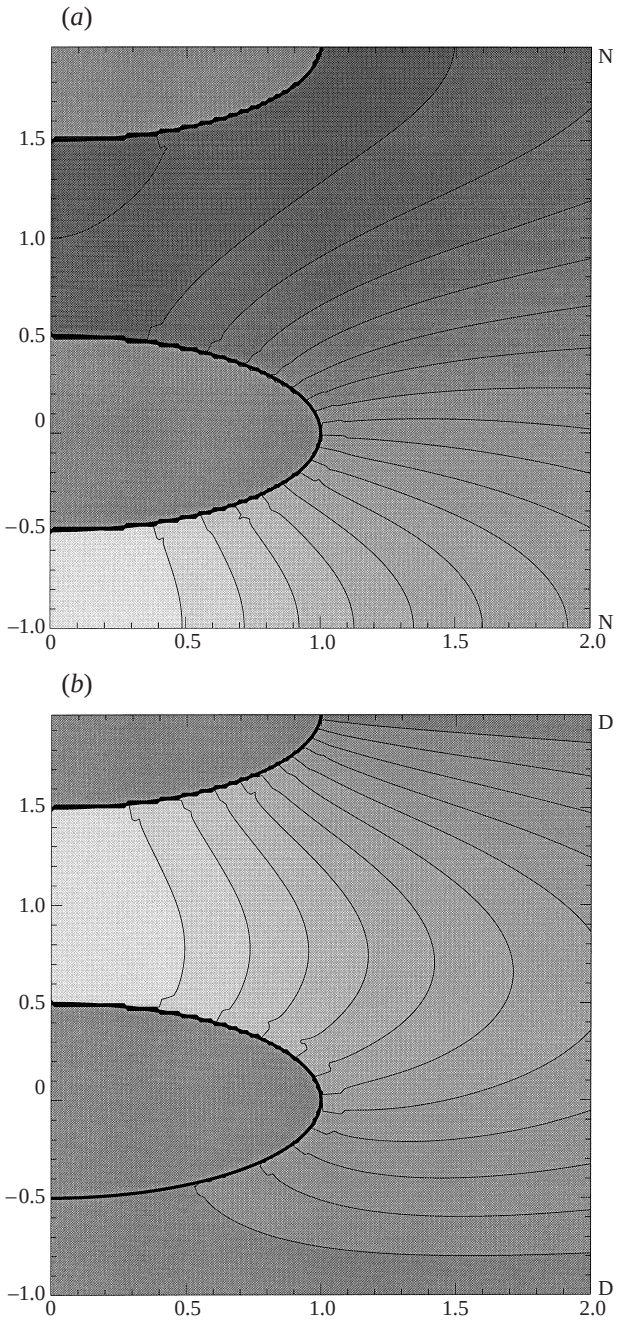

FIGURE 6. The field in the lower-right-hand quadrant of (*a*) a Neumann and (*b*) a Dirichlet trapped mode about three elliptical cylinders, $b/a = \frac{1}{2}$, $a/d = 1$, corresponding to $\beta d = \frac{1}{3}\pi$, occurring at $kd = 0.9298$.

this section we focus on this value of $\beta d = \frac{1}{2}\pi$, and consider unsymmetric cylinder cross-sections. In the previous section the case of $\beta d = \frac{1}{2}\pi$ with symmetric cylinder cross-sections was shown to correspond to antisymmetric trapped modes in a parallel straight-walled Neumann waveguide. Evans *et al.* (1994) have shown that these

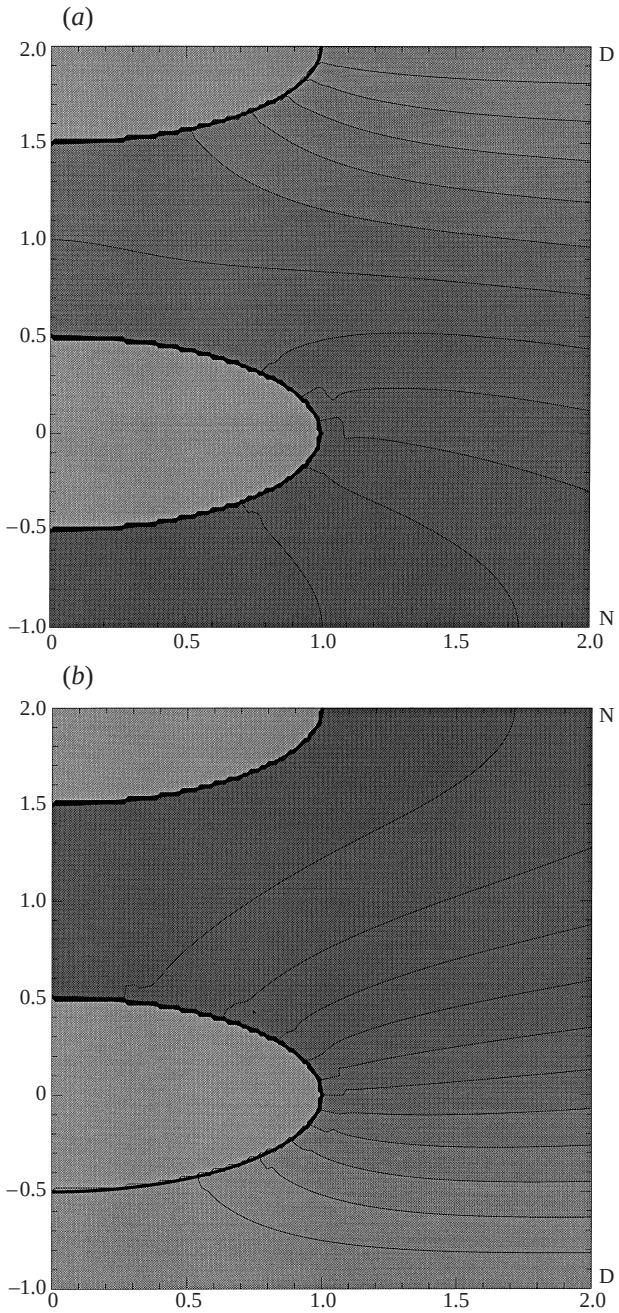

FIGURE 7. The field in the lower-right-hand quadrant of (*a*) a Neumann and (*b*) a Dirichlet trapped mode about three elliptical cylinders, $b/a = \frac{1}{2}$, $a/d = 1$, corresponding to $\beta d = \frac{1}{6}\pi$, occurring at $kd = 0.5125$.

trapped modes exist for all symmetric cylinder cross-sections. However in the absence of symmetry all that can be deduced from the choice of $\beta d = \frac{1}{2}\pi$ is that the Rayleigh–Bloch mode has period $2d$. We can therefore expect, using continuity arguments, that a smooth perturbation from a symmetric to an unsymmetric cross-section will lead to

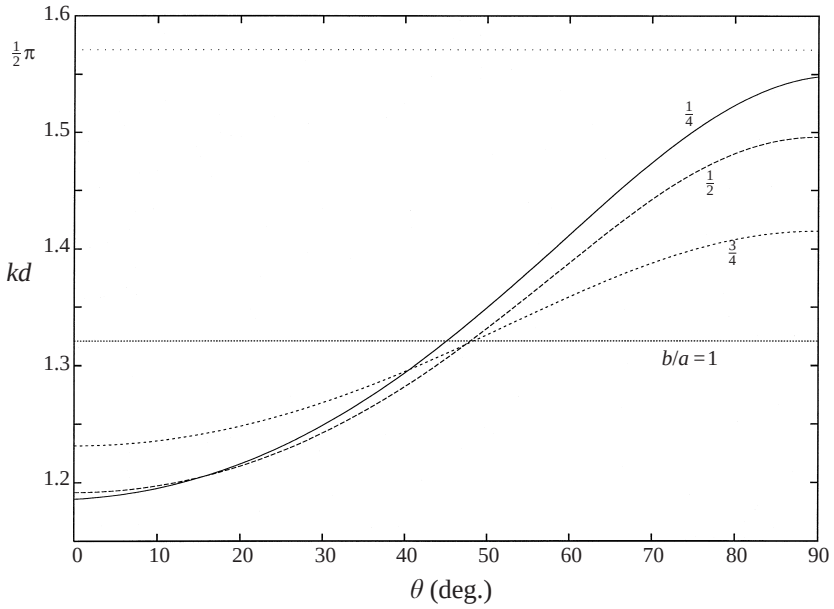

FIGURE 8. The variation of wavenumber kd when $\beta d = \frac{1}{2}\pi$ as an elliptical cylinder with $a/d = \frac{4}{5}$ and various aspect ratios (shown against curves) is rotated through an angle θ.

a smooth shift in the position of the zero of the determinant and hence in kd and a smooth distortion of the parallel-sided walls from $y = \pm d$. This is indeed what turns out to be the case as our numerical examples will show.

As a first example, we consider a cylinder of fixed elliptical cross-section and rotate it through an angle θ with respect to the centreline (see equation (3.12)). Curves showing variation of the wavenumber kd with θ for $\beta d = \frac{1}{2}\pi$ are presented in figure 8 for four cross-sections having the same 'length' $a/d = \frac{4}{5}$, but aspect ratios of $b/a = 1$, $\frac{3}{4}$, $\frac{1}{2}$ and $\frac{1}{4}$. The first of these is just a circular cylinder and does not vary with θ. For $\theta = 0^\circ$ and 90° the solution refers to the antisymmetric trapped mode in a straight-walled channel as discussed above where existence is guaranteed. In between these two limits the geometry is unsymmetric and the wavenumber moves smoothly from one limit to the other. Although the numerical method prohibits calculations for thin geometries such as flat plates, we can use the convergence of the results seen in figure 1 for a series of thinning ellipses to those for an equivalent thin plate to surmise that these special Rayleigh–Bloch surface waves with $\beta d = \frac{1}{2}\pi$ also exist for an infinite periodic array of thin tilted parallel plates. Furthermore, the results for $b/a = \frac{1}{4}$ in figure 8 are probably a good approximation to the wavenumbers for Rayleigh–Bloch modes about arrays of tilted thin plates. Note however that such Rayleigh–Bloch modes do not exist if the plates are aligned with each other ($\theta = 90^\circ$) as in a perforated diffraction screen.

In figure 9 we have plotted the field lines in the vicinity of an elliptical cylinder ($a/d = \frac{3}{4}$, $a/b = \frac{2}{3}$, $\theta = 45^\circ$) and labelled the lines upon which Neumann (N) and Dirichlet (D) conditions are satisfied. It can be seen that by replacing the dotted lines by rigid walls, this particular Rayleigh–Bloch mode can be regarded as a trapped mode about an unsymmetric cylinder in a channel of width $2d$ having distorted walls. At either infinity the mode asymptotes to a straight-walled waveguide with a Dirichlet condition on its centreline, although these asymptotes at $x = \pm\infty$ do not correspond

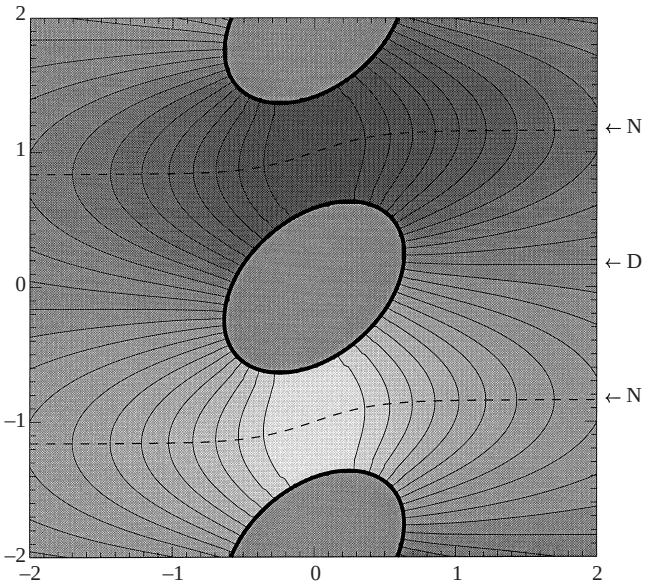

FIGURE 9. The field lines for a Rayleigh–Bloch mode with $\beta d = \frac{1}{2}\pi$ in the presence of a periodic array of elliptical cylinders, $b/a = \frac{2}{3}$, $\theta = 45^\circ$. Dashed line corresponds to the line on which normal velocity vanishes.

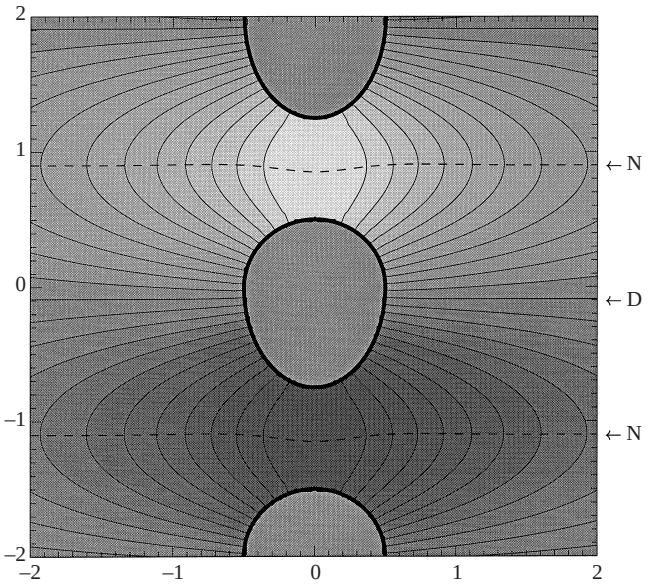

FIGURE 10. The field lines for a Rayleigh–Bloch mode with $\beta d = \frac{1}{2}\pi$ in the presence of a periodic array of unsymmetric cylinders; top half-circle, radius $a/d = \frac{1}{2}$, bottom half, ellipse with $b/a = \frac{3}{2}$. Dashed line corresponds to the line on which normal velocity vanishes.

to the same values of y. This trapped mode in a parallel but distorted channel or waveguide is a new addition to our catalogue of trapped modes and adds weight to the conjecture that no trapped mode exists in the presence of an unsymmetric cylinder on the centreline of a channel of rectangular cross-section.

When the cylinder array is symmetric about a line through the cylinders, as in

Geometry	kd (trapped mode)	kd (peak force)	Maximum non-dimensional force on middle cylinder
$b/a = \frac{1}{2}$	1.4102	1.4005	9.7
$b/a = \frac{3}{2}$	1.3835	1.3760	10.0

TABLE 3. Comparison of trapped mode wavenumber with the wavenumber at which the maximum force is experienced in an array of 25 cylinders having a circular upper cross-section $a/d = \frac{1}{2}$ and an elliptical lower cross-section $(x/a)^2 + (y/b)^2 = 1$.

figure 10, the waveguide asymptotes to the same values of y despite some local distortion to accommodate the lack of symmetry in the cross-section. In figure 10 we have chosen a cylinder cross-section which consists of a circular upper-half ($a/d = \frac{1}{2}$) and an elliptical lower half ($a/d = \frac{1}{2}$, $b/a = \frac{3}{2}$).

It was found that for every example of cylinder cross-section computed numerically by the authors, a zero of determinant, and hence a Rayleigh–Bloch mode with $\beta d = \frac{1}{2}\pi$ exists. It is therefore tempting to conclude that arrays of identical cylinders of arbitrary cross-section will support these new trapped modes in distorted channels or waveguides.

The importance of the occurrence of trapped modes about symmetric cylinders in both Neumann and Dirichlet waveguides has been brought into focus by Maniar & Newman (1997) who showed that large forces are experienced by cylinders in a finite periodic array of such cylinders in an incident wave field. In the light of the results from this section, we can now expect similar large forces in the case of wave interaction with a finite periodic array of unsymmetric bodies. J. N. Newman (personal communication) has computed the first-order forces on a finite array of unsymmetric cylinders using a wave interaction program HIPAN. Two sets of results for arrays of 25 cylinders consisting of hybrid cylinder cross-sections of the type shown in figure 10 are shown in table 3. It can be seen that the difference between the resonant wavenumber at which the largest force on the middle cylinder of an array of 25 cylinders, non-dimensionalized with respect to the force on an isolated cylinder, occurs and the actual Rayleigh–Bloch mode wavenumber, is small and in fact is comparable to similar results for arrays of symmetric bodies (Maniar & Newman 1997). Finally, it should be noted that no solutions have been found for unsymmetric cylinder cross-section at values of Rayleigh–Bloch wavenumbers, βd, other than $\frac{1}{2}\pi$, due to the complex nature of the determinant.

6. Conclusion

In this paper, we have been concerned with computing solutions for Rayleigh–Bloch surface waves along an infinite periodic grating consisting of identical cylinders of uniform cross-section. We have also determined, numerically, what types of cylinder cross-sections can support Rayleigh–Bloch waves. These localized surface waves are described by a wave progressing along the grating with a dominant Rayleigh–Bloch wavenumber, β, related to the change in phase from one cylinder to the next. Simple arguments show that the periodicity in the geometry induces a cut-off frequency below which a wave cannot radiate to infinity, and so the problem is reduced to finding real values of wavenumber k such that $k < \beta$. The problem is formulated using Green's Identity with an appropriate Green function to construct an integral

equation, whose approximate solution is sought by discretization and collocation. Rayleigh–Bloch solutions are then determined by the real values of k such that the determinant of the resulting complex system of equations vanishes. It was shown that if each cylinder cross-section is symmetric about a line through it perpendicular to the line containing all the cylinders in the grating the determinant of the system is real. Results were presented for a range of such symmetric cylinder cross-sections. It was also shown that by choosing particular values of β, the problem could be interpreted as representing the trapped modes about any number of cylinders periodically spaced across a waveguide or channel. Thus, curves such as those shown in figures 1 and 2 become extremely important in that they can be used to determine the frequencies of trapped modes in the presence of any number of cylinders in a channel. The use of a Rayleigh–Bloch approach to the problem provides confidence in seeking the existence of such modes, all of which occur below the Rayleigh–Bloch cut-off $k < \beta$ despite being above the corresponding cut-off for the waveguide. Rayleigh–Bloch theory also enables us to conclude that there exist N trapped modes in a Neumann waveguide containing N cylinders and at most N trapped modes in a Dirichlet waveguide. Of particular interest was the conclusion that Neumann trapped modes exist for any odd number of identical symmetric cylinders spanning a waveguide and having a Neumann condition on the centreline in contrast to the case of a single cylinder on the centreline.

For the special value of $\beta = \pi/2d$, where $2d$ is the separation between cylinders in the array, it was shown that Rayleigh–Bloch surface waves are supported by cylinders having arbitrary cross-sections and correspond to non-progressive or standing modes. They provide new examples of trapped modes about unsymmetric cylinders in distorted parallel channels or waveguides.

Rayleigh–Bloch surface waves are of importance in many fields of study, though we have concentrated on the context of water waves here. In particular, Maniar & Newman (1997) have shown how large forces and amplitudes can develop at frequencies close to the trapped mode frequencies described here in the case of a finite array of cylinders in the presence of a source of excitation such as an incident wave field. We have now extended this to show that finite arrays of unsymmetric cylinders will be subject to similar resonances. In the context of acoustics, we can now predict resonant or trapped modes wavenumbers for either acoustically hard or soft lined parallel waveguides containing a cascade of cylinders similar to those reported by Parker & Stoneman (1989) for a cascade of thin plates.

There are still issues that need resolving. For example, do trapped modes exist about multiple cylinders spanning a waveguide when they are not arranged in such a way that they form part of an infinite array as described here? For two cylinders placed symmetrically about the centre of the waveguide, Davies & Parnovski (1998) provide different conditions under which they do and do not exist.

In work on the scattering theory for diffraction gratings, Wilcox (1984, p. 12) states that no general criteria are known for the existence of Rayleigh–Bloch surface waves satisfying a Neumann condition on the gratings. The numerical computations presented here suggest that Rayleigh–Bloch waves exist near gratings formed by any symmetric cross-section, and it may be possible to extend the work of Evans *et al.* (1994) to provide a rigorous proof of this. The existence of Rayleigh–Bloch waves above the cut-off frequency is unlikely apart from the special cases of $\beta d = \frac{1}{2}\pi$ and $\beta d = \pi$. See, for example, Evans & Porter (1998).

R.P. would like to acknowledge the support of EPSRC research grant no. GR/K67526. The authors would also like to thank Dr D. Porter for useful discussions.

REFERENCES

Callan, M., Linton, C. M. & Evans, D. V. 1991 Trapped modes in two-dimensional waveguides. *J. Fluid Mech.* **229**, 51–64.

Davies, E. B. & Parnovski, L. 1998 Trapped modes in acoustic waveguides. *Q. J. Mech. Appl. Maths* **51**, 477–492.

Evans, D. V. & Fernyhough, M. 1995 Edge waves along periodic coastlines. Part 2. *J. Fluid Mech.* **297**, 307–325.

Evans, D. V. & Kuznetsov, N. 1998 Trapped Modes. In *Advances in Fluid Mechanics: Gravity Waves in Water of Finite Depth* (ed. J. N. Hunt). Computational Mechanics Southampton.

Evans, D. V., Levitin, M. & Vassiliev, D. 1994 Existence theorems for trapped modes. *J. Fluid Mech.* **261**, 21–31.

Evans, D. V. & Linton, C. M. L. 1993 Edge waves along periodic coastlines. *Q. J. Mech. Appl. Maths* **46**, 644–656.

Evans, D. V. & Porter, R. 1997 Trapped modes about multiple cylinders in a channel. *J. Fluid Mech.* **339**, 331–356.

Evans, D. V. & Porter, R. 1998 Trapped modes embedded in the continuous spectrum. *Q. J. Mech. Appl. Maths* **51**, 263–274

Linton, C. M. 1998 The Green's function for the two-dimensional Helmholtz equation in periodic domains. *J. Engng Mech.* **33**, 377–402.

Linton, C. M. & Evans, D. V. 1992 Integral equations for a class of problems concerning obstacles in waveguides. *J. Fluid Mech.* **245**, 349–365.

Maniar, H. D. & Newman, J. N. 1997 Wave diffraction by a long array of cylinders. *J. Fluid Mech.* **339**, 309–330

McIver, M. & Linton, C. M. 1995 On the non-existence or otherwise of trapped modes in acoustic waveguides. *Q. J. Mech. Appl. Maths* **48**, 543–555.

McIver, P., Linton, C. M. & McIver, M. 1998 Construction of trapped modes for waveguides and diffraction gratings. *Proc. R. Soc. Lond.* A **454**, 2593–2616.

Parker, R. & Stoneman, S. A. T. 1989 The excitation and consequences of acoustic resonances in enclosed fluid flow around solid bodies. *Proc. Inst. Math. Engrs* **203**, 9–19.

Stokes, G. G. 1846 Report on recent researches in hydrodynamics. *Brit. Ass. Rep.*

Utsunomiya, T. & Eatock Taylor, R. 1998 Analogies for resonances in wave diffraction problems *Proc. 13th Intl Workshop on Water Waves and Floating Bodies, Delft, The Netherlands.*

Wilcox, C. H. 1984 *Scattering Theory for Diffraction Gratings.* Springer.